

**Book chapter in**  
***Introduction to Complex Mediums for Optics and Electromagnetics***

Editors: Werner S. Weiglhofer & Akhlesh Lakhtakia

*SPIE Optical Engineering Press, 2003*

**Magnetoimpedance in multilayered films for miniature  
magnetic sensors**

Larissa V. Panina and Dmitriy P. Makhnovskiy  
Department of Communication and Electrical Engineering,  
University of Plymouth, Drake Circus, Plymouth PL4 8AA, Great Britain.

**Abstract**

The discovery of the magnetoimpedance (MI) effect in 1994 had a strong impact on the development of micro magnetic sensors operating at nano-Tesla range. In certain soft magnetic materials, such as composites of amorphous thin wires, the impedance change (MI ratio) is in the range of 50-100 % in the MHz frequency band for external magnetic fields of few Oe. However, when decreasing the size of the sensor element, the maintenance of such high sensitivity becomes a major concern. Special thin-film structures have been proposed and fabricated to improve the MI performance in miniature elements. This chapter concerns the principal advantages of MI in magnetic/metallic multilayered materials and their applications to magnetic sensing technology. Physical concepts, theoretical analysis based on the field-dependent surface impedance matrix, experimental results, and sensor designs are discussed. These encompass multi-fold enhancement of the MI ratio, a considerable extension of the operational frequency range, and the field symmetry of the MI behavior. Layered systems allow special types of magnetic anisotropy (either transverse or crossed) to be established in order to realize antisymmetric and asymmetric MI effects. This property is of a particular interest for magnetic-sensor applications.

## 1 Introduction

Miniature magnetic-sensor technology is a rapidly growing industry. Sensitive and rapid-response sensors are in great demand for advanced intelligent measurement and control systems. This demand has been satisfied in some areas by magneto-resistance (MR), giant magneto-resistance (GMR), fluxgate and other technologies [1]-[3]. A relatively new magnetic sensor technology based on the magnetoimpedance (MI) effect has the potential to overtake some of the other emergent sensor systems in term of performance and low cost [4]-[6]. MI sensors combine such desirable characteristics as high sensitivity, miniature size, fast response, and low power consumption, which make them unique in the magnetic sensor family.

The MI sensing performance is based on enormous changes in the complex-valued impedance at high frequencies under the application of a dc (or low frequency) magnetic field [7]-[12]. The ratio of the percent change of the impedance, called the MI ratio, reaches the value up to 150 % at MHz frequencies in amorphous micro wires having circumferential (or helical) anisotropy. The characteristic magnetic fields required to cause this impedance change are in the range of 1-5 Oe. Then, MI sensitivity is at least one order of magnitude higher than that of GMR materials. However, the MI-wires have much greater dimensions: 10-50 micron in diameter and a few mm in length. With decreasing sensor-element size, the maintenance of ultra high sensitivity becomes a problem. Special thin-film structures are employed to improve the MI performance in miniature elements (thickness  $< 1 \mu\text{m}$ , in-plane size  $< 200 \mu\text{m}$  and length  $< 5000 \mu\text{m}$ ) [14]-[17].

This chapter deals with MI in sandwich-type structures having two outer magnetic layers and an inner conductive lead. The MI ratio in these systems has been proven to be much greater than in a similar ferromagnetic single-layer. For example, in CoFeSiB/Cu/CoFeSiB multilayers of several micrometers thickness the impedance change is more than 300% at 10 MHz under the application of a dc magnetic field of about 10 Oe [14]. In contrast, a single CoFeSiB layer under the same conditions exhibits just a few percent change.

In electrically uniform materials subjected to a dc magnetic field, MI originates from the dependence of the skin depth on the transverse permeability. In multilayer structures having a highly conductive inner film, a very large change in impedance can occur at quite low frequencies when the inductance caused by the outer magnetic layers becomes sufficiently high. This results in multi-fold enhancement of the MI ratio and a considerable extension of the operational frequency range. Furthermore, special types of magnetic anisotropy can be realized in layered systems [18]-[20]. Multilayers with a transverse anisotropy produce antisymmetric response manifested as off-diagonal terms in the surface impedance tensor. Cross-anisotropy films exhibit asymmetric MI characteristics. These features are crucially important to obtain a linear voltage response with enhanced sensitivity, without requiring large power consumption, and are of particular interest for magnetic-sensor applications.

## 2 Analysis of MI in multilayer structures

In this section, we discuss a symmetrical 3-layer film model that reflects all the essential feature of MI behavior in multilayered materials. We start our analysis with considering the impedance  $Z$  of this structure in a usual way as the ratio  $Z = V_f / i$ , where  $V_f$  is the voltage induced in the film by a passing current  $i$ . However, in a magnetic system the induced voltage can be of a more complicated origin. For example, the voltage  $V_f$  can be induced by the current  $i_c$  flowing in the coil attached to the film. Alternatively, the current  $i$  is capable of generating the coil voltage  $V_c$ . To describe the generalized voltage ( $V_f, V_c$ ) as response to excitation ( $i, i_c$ ) it is convenient to introduce the surface impedance tensor  $\hat{\zeta}$ . We calculate the tensor  $\hat{\zeta}$  in the low frequency approximation, which neglects the skin effect. This approach is reasonable for not very thick films ( $< 1 \mu\text{m}$ ) and for not very high frequencies ( $< 1 \text{ GHz}$ ), which covers a wide range of applications. Nevertheless, the approach to the exact solution is considered as well. Finally, the effect of the film in-plane size on MI is analyzed. Gaussian units are used since they are more convenient in electromagnetics.

The structure consists of an inner conductive lead (M) of a thickness  $2d_1$  and two identical magnetic layers (F) of a thickness  $d_2$  along the  $x$  axis. The layers are parallel to the  $yz$  plane having a width  $b$  ( $y$  axis) and length  $l$  ( $z$  axis). An external dc magnetic field  $H_{\text{ex}}$  (which is to be sensed) is applied parallel to the  $z$  axis. In general, a dc bias current  $I_b$  can be also used to modify the static magnetic structure. This model is depicted in Figure 1.

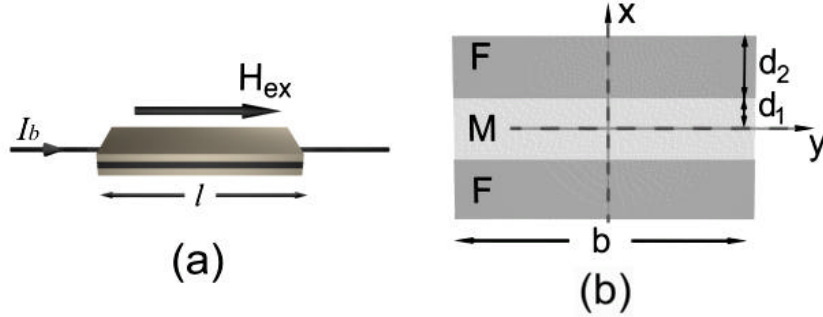


Figure 1. Schematic drawing of 3-layer MI film showing principal directions and quantities used. (a): general view, (b): cross-section of the film.

Although the magnetic layers are made of the same alloy, they can be produced with different magnetic anisotropy. In particular, we are interested in the case when the anisotropy axes are directed at an angle  $\pm\alpha$  to the  $z$  axis, respectively for the upper ( $x > 0$ ) and lower ( $x < 0$ ) magnetic layers. Such anisotropy can be induced, for example, by current annealing in the presence of a longitudinal field. The combination of anisotropy,  $H_{\text{ex}}$  and

$I_b$  which induces a circulatory magnetic field  $H_b(x > 0) = -H_b(x < 0)$  results in the antisymmetric arrangement of dc magnetization  $\mathbf{M}_0$  such that  $M_{0y}(x > 0) = -M_{0y}(x < 0)$ .

## 2.1 Impedance of symmetrical 3-layer film

Our first goal is to calculate the impedance of 3-layer structure shown in Figure 1, when it is excited by an alternating current  $i = i_0 \exp(-j\omega t)$  flowing along the  $z$  axis. The layer thicknesses  $d_1$  and  $d_2$  are such that the skin effect can be neglected. If the inner lead conductivity  $\sigma_1$  is considerably higher than the conductivity  $\sigma_2$  of the magnetic layers (to be exact,  $\sigma_1 d_1 \gg \sigma_2 d_2$ ), the current mainly flows along the conductive lead. With these assumptions, the expression for the impedance can be written in the form:

$$Z = R_m - j\omega\Phi/ci, \quad (1)$$

where  $R_m = l/2\sigma_1 d_1 b$  is the resistance of the inner conductor,  $\Phi$  is the total transverse magnetic flux generated by the driving current  $\mathbf{i}$  in the magnetic layers, and  $c$  is the velocity of light. If the edges effects are neglected (i.e., the film is treated as infinitely long in the  $y$  and  $z$  directions) the ac magnetic field  $\mathbf{h}$  in the magnetic layers is uniform. Then:

$$\Phi = (\hat{\boldsymbol{\mu}}\mathbf{h})_y d_2 l, \quad (2)$$

where  $\hat{\boldsymbol{\mu}}$  is the ac permeability tensor. In general, the field  $\mathbf{h}$  has  $y$ - and  $x$ -components due to the tensor form of the permeability. The value of the  $y$ -component is related to the current as  $|h_y| = 2\pi i / cb$ , and the relation between  $h_y$  and  $h_x$  is determined from the condition that the normal magnetic flux is zero (i.e.,  $(\hat{\boldsymbol{\mu}}\mathbf{h})_x = 0$ ); accordingly:

$$\Phi = \tilde{\mu}_{yy} h_y d_2 l = \tilde{\mu}_{yy} d_2 \frac{2\pi i l}{cb}, \quad (3)$$

$$\tilde{\mu}_{yy} = \mu_{yy} + \mu_{xy}^2 / \mu_{xx}.$$

After using (3), the impedance can be written in the form:

$$Z = R_m \left( 1 - 2j\tilde{\mu}_{yy} \frac{d_1 d_2}{\delta_1^2} \right), \quad (4)$$

where  $\delta_1 = c/\sqrt{2\pi\sigma_1\omega}$  is the skin depth in the metallic inner lead. Expression (4) shows that the MI ratio in the sandwich film can be very large even at relatively low frequencies when the skin effect is not substantial, and has a linear dependence on  $\tilde{\mu}_{yy}$ .

This conclusion can be illustrated as follows. At a frequency of 10 MHz, taking  $d_1 = d_2 = 0.5 \mu\text{m}$  and  $\sigma_1 = 2 \cdot 10^{18} \text{s}^{-1}$  (conductivity of copper), we get  $d_1/\delta_1 = d_2/\delta_1 = 0.045$ . A typical low-frequency change in the permeability  $\tilde{\mu}_{yy}$  (having a rotational mechanism) under the application of  $H_{\text{ex}} \cong H_K$  (where  $H_K$  is the effective anisotropy field) is from 1 to 500; then, the impedance varies over 200 % according to (4).

The impedance for the present geometry can be calculated exactly for any frequency, without neglecting the skin effect [18]-[21]. For a film of  $1 \mu\text{m}$  thickness with  $\sigma_1 d_1 / \sigma_2 d_2 \approx 50$  (as for a CoSiB/Cu/CoSiB system with amorphous magnetic films), the approximate solution almost coincides with the exact one up to a frequency of 1 GHz.

## 2.2 Surface impedance tensor

For the considered configuration, the ac current induces both the voltage  $V_f$  between the film ends and the coil voltage  $V_c$ , as shown in Figures 2a and 2b, since the current flow gives rise to an antisymmetric transverse magnetization (or circulatory magnetization) and a non-zero longitudinal magnetization.

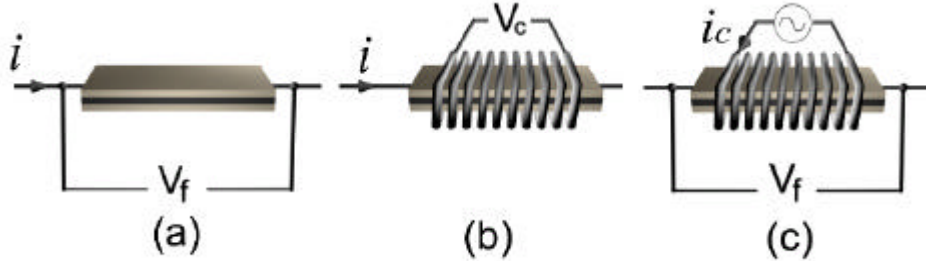


Figure 2. Methods of ac voltage excitation.

If the film is placed in a variable longitudinal field  $h_{\text{ex}}$  induced by the coil current  $i_c$ , not only the longitudinal magnetization is induced, but also the circulatory magnetization contributing to  $V_f$ , as shown in Figure 2c. A mixed excitation by both the current  $i$  in the film and current  $i_c$  in the coil can be used. The crossed magnetization processes related to the voltages  $V_c$  and  $V_f$  are known as the inverse Wiedemann and the Matteucci effects [6]. With increasing frequency, the induced voltages become of the same order and very sensitive to the longitudinal field  $H_{\text{ex}}$ .

The induced voltages are convenient to describe in terms of the surface impedance tensor  $\mathbf{\zeta}$  [13, 18, 20] that relates the variable electric  $\mathbf{e}_t$  and magnetic  $\mathbf{h}_t$  fields taken on the external surfaces  $x = \pm d$  ( $d = d_1 + d_2$ ). Thus:

$$e_{t\alpha} = \zeta_{\alpha\beta} (\mathbf{h}_t \times \mathbf{n})_\beta, \quad \alpha, \beta = z, y, \quad (5)$$

where  $\mathbf{n}$  is a unit vector directed inside the film, while  $\mathbf{e}_t$  and  $\mathbf{h}_t$  are tangential to the surface. The voltage  $V_f$  is determined by the surface value of the longitudinal electric field  $e_z(d) = e_z(-d)$  and is related to the fields  $h_y$  and  $h_z = h_{ex}$  via the components  $\zeta_{zz}$  and  $\zeta_{zy}$  as follows:

$$V_f = (\zeta_{zz} h_y - \zeta_{zy} h_{ex}) l, \quad (6)$$

$$h_y = (2\mathbf{P}/cb)i, \quad h_{ex} = 4\pi n_1 i_c / c, \quad (7)$$

where  $n_1$  is the number of turns per unit length in the excitation coil. The coil voltage  $V_c$  is associated with the circulatory electric field  $e_y(d) = -e_y(-d)$  and can be expressed as:

$$V_c = 2bN_2 (\zeta_{yz} h_y - \zeta_{yy} h_{ex}), \quad (8)$$

where  $N_2$  is the number of turns in the detection coil. In a general case, two coils can be used: the excitation coil for producing  $h_{ex}$  and the pick-up coil for detection of  $V_c$ . Equations (6) and (8) can be written in terms of currents  $i$  and  $i_c$ :

$$\begin{pmatrix} V_f / l \\ V_c / 2bN_2 \end{pmatrix} = \begin{pmatrix} \zeta_{zz} & -\zeta_{zy} \\ \zeta_{yz} & -\zeta_{yy} \end{pmatrix} \begin{pmatrix} Ai \\ Bi_c \end{pmatrix}, \quad (9)$$

where the parameters  $A = h_y / i$  and  $B = h_{ex} / i_c$  are given by (7).

The surface impedance tensor can be easily found in the low-frequency approximation. Here we are interested in analyzing  $\zeta_{zz}$  and  $\zeta_{yz} = \zeta_{zy}$  components. The parameter  $\zeta_{zz}$  is obtained by comparing (4) and (9) wherein  $i_c = 0$ :

$$\zeta_{zz} = Z / A = \zeta_0 (1 - 2j\tilde{\mu}_{yy} \frac{d_1 d_2}{\delta_1^2}), \quad \zeta_0 = \frac{c}{4\pi\sigma_1 d_1}. \quad (10)$$

The off-diagonal component, say  $\zeta_{yz}$ , can be found by considering the coil voltage  $V_c$  induced by the film current  $i$ . This voltage is related to the longitudinal magnetic flux:

$$V_c = -j\omega N_2(2d_2b)(\hat{\mu}h)_z. \quad (11)$$

When comparing (11) and (9) taken with  $i_c = 0$  one can obtain:

$$\begin{aligned} \zeta_{yz} &= V_c / 2bN_2Ai = -j\omega d_2 \tilde{\mu}_{zy} / c, \\ \tilde{\mu}_{zy} &= \mu_{zy} - \mu_{zx}\mu_{xy} / \mu_{xx}. \end{aligned} \quad (12)$$

### 2.3 Exact solution for the surface impedance tensor.

The calculation of  $\hat{\zeta}$  valid for any frequency is based on the solution of the Maxwell equations for the fields  $\mathbf{e}$  and  $\mathbf{h}$ , together with the equation of motion for the magnetization vector  $\mathbf{M}$ . The theoretical aspects of the problem can be very complicated and generally require approximations. Typically, a linear approximation with respect to the time-variable parameters  $\mathbf{e}$ ,  $\mathbf{h}$  and  $\mathbf{m} = \mathbf{M} - \mathbf{M}_0$  (where  $\mathbf{M}_0$  is the static magnetization) is used. On assuming a local relationship between  $\mathbf{m}$  and  $\mathbf{h}$  ( $\mathbf{m} = \hat{\chi} \mathbf{h}$ ), the problem is simplified to finding the solutions of Maxwell's equations with a given ac permeability tensor  $\hat{\mu} = 1 + 4\pi\hat{\chi}$ , which corresponds to neglecting the exchange effects.

Further assumptions about  $\hat{\mu}$  are needed. The permeability depends on many factors, including the domain configuration, anisotropy and stress distribution, and the mode of magnetization (domain wall motion or magnetization rotation). These factors can be very complicated in real materials, making modeling very difficult. The problem is simplified if the domain structure is not considered (in practice, it can be eliminated by a proper dc bias) and if  $\mathbf{M}_0$  is constant in the films. Then,  $\hat{\mu}$  is determined by the magnetic moment rotation and is independent of the position. Furthermore, the tensor  $\hat{\mu}$  has a general form that reduces to a quasi-diagonal form in the primed co-ordinate system with the axis  $z' \parallel \mathbf{M}_0$ , shown in Figure 3.

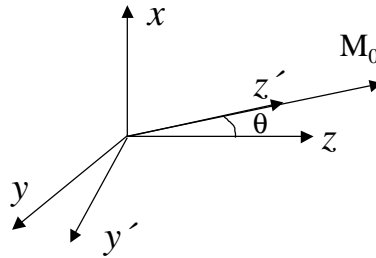


Figure 3. Original  $xyz$  and primed  $x'y'z'$  co-ordinate systems. Using primed coordinates reduces the permeability tensor to quasi-diagonal form.

In the case of a uniform precession of the total magnetization vector  $\mathbf{M}$  around  $\mathbf{M}_0$ , the susceptibility tensor in the primed coordinates  $(x, y', z')$  is of the form:

$$\hat{\chi} = \begin{pmatrix} \chi_1 & -j\chi_a & 0 \\ j\chi_a & \chi_2 & 0 \\ 0 & 0 & 0 \end{pmatrix}. \quad (13)$$

This form can be easily obtained from the linearized Landau-Lifshitz equation describing the magnetization dynamics. The expressions for  $\chi_1$ ,  $\chi_2$ ,  $\chi_a$  depend on a the specific magnetic configuration [19].

Here we are restricted to the consideration of magnetization rotation dynamics only, assuming that the domain wall displacements are strongly damped. Then, (13) determines the permeability tensor  $\hat{\mu} = 1 + 4\pi\hat{\chi}$ . To calculate the normalized parameters  $\tilde{\mu}_{yy}$  and  $\tilde{\mu}_{zy}$  which appear in expressions (10) and (12) for the impedance components, the tensor  $\hat{\mu}$  has to be written in the original coordinates  $x, y, z$ , which yields:

$$\tilde{\mu}_{yy} = 1 + 4\pi\chi\cos^2\theta, \quad (14)$$

$$\tilde{m}_{zy} = -4\mathbf{p}\mathbf{c}\sin\mathbf{q}\cos\mathbf{q}, \quad (15)$$

$$\chi = \chi_2 - \frac{4\pi\chi_a^2}{1 + 4\pi\chi_1},$$

where  $\mathbf{q}$  is the angle between the dc magnetization  $\mathbf{M}_0$  and the  $z$  axis.

#### 2.4 MI in a narrow sandwich (width effect)

For a practical device use, the effect of in-plane sandwich width on MI has to be studied. If the edge effect is neglected (approximation of an infinite width), the magnetic flux generated by the current flowing along the inner lead is confined within the outer magnetic layers. In a sandwich of finite width, the flux leaks across the inner conductor [21], [22], [24]. This process eventually results in the considerable drop in MI ratio, if the film width is smaller than some critical value depending on the transverse permeability and the thicknesses of the magnetic and conductive layers. This process is similar to that resulting in a drop in the efficiency of inductive recording heads [25], [26].

The effect of the flux leakage across the conductive layer is found to be described by an effective ‘‘ac demagnetizing’’ factor  $g$  that reduces the permeability and makes it less sensitive to the dc field  $H_{ex}$  when the film width  $b$  is decreased. In the low-frequency approximation when the skin effect is neglected the parameter  $g$  is given by:

$$g(k) = \frac{1}{(k_1\lambda)^2} \left( 1 - (k\lambda)^2 \frac{kb \sinh kb}{kb \sinh kb + 2(k_1\lambda)^2(1 - \cosh kb)} \right), \quad (16)$$

$$k^2 = 1/\lambda^2 - k_1^2, \quad \lambda^2 = d_1 d_2 \tilde{\mu}_{yy}, \quad k_1 = (1+j)/\delta_1.$$

For  $kb \gg 1$  (or  $b/I \gg 1$ ) the function  $g$  tends to be unity. It means that the parameter  $b^* = 1/k$  plays the role of a critical width: for  $b < b^*$  all the film dimensions  $b$ ,  $d_1$  and  $d_2$  influence the value of the impedance. In the low-frequency limit,  $b^* = \sqrt{d_1 d_2 \tilde{\mu}_{yy}}$ . Typical parameters for the structures of interest are  $d_1 \approx d_2 \approx 0.1-0.5 \mu\text{m}$ ,  $2b \approx 10-50 \mu\text{m}$  and  $\mu_t \approx 10^3$ , for which  $b^* \approx 3-15 \mu\text{m}$  is comparable to the half-width, which means that the size effects can not be neglected.

Figure 4 shows the plots of the impedance change vs. frequency with the film width  $b$  as a parameter for magnetic films with transverse anisotropy [21].

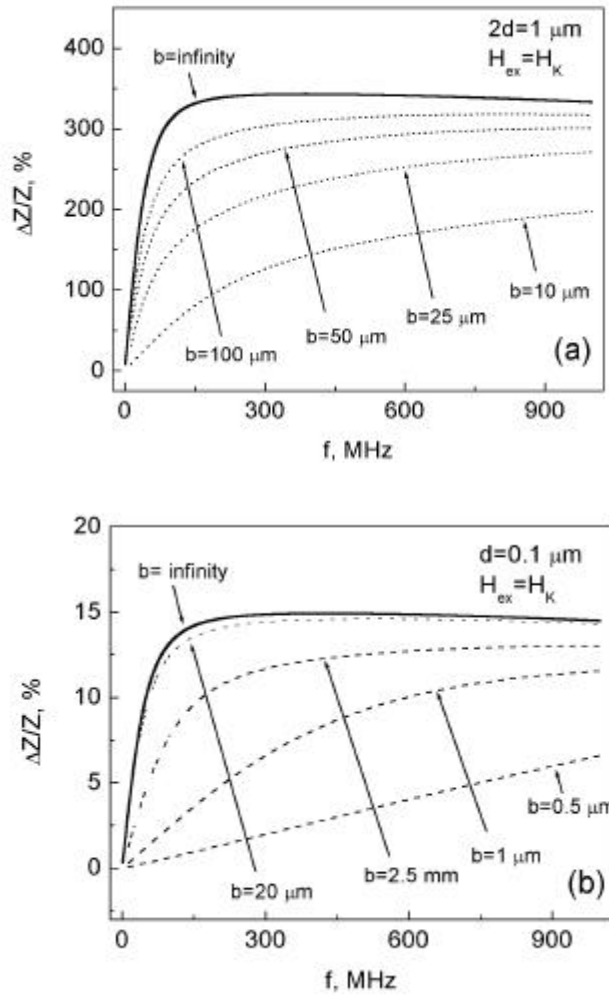


Figure 4. Maximum impedance change ratio  $\Delta Z/Z = |(Z(H_K) - Z(0))/Z(0)|$  in a sandwich structure with transverse anisotropy as a function of frequency with the width  $b$  as a parameter.  $d_1 = d_2 = 0.25 \mu\text{m}$  in (a) and  $d_1 = d_2 = 0.05 \mu\text{m}$  in (b).

It is convenient to define the impedance change ratio as  $\Delta Z/Z = |Z(H_K) - Z(0)|/|Z(0)| \cdot 100\%$ , where  $H_K$  is the anisotropy field (for transverse anisotropy and  $I_b = 0$ , the magnetic layers are magnetized along the  $z$  axis when  $H_{ex} = H_K$ ). The function  $|Z(H_{ex})|$  has a maximum at  $H_{ex} \approx H_K$ , associated with that for the rotational transverse permeability  $\tilde{\mu}_{yy}$ . Therefore, the introduced parameter gives the maximum impedance change. The magnetic and electric parameters taken for the calculations correspond to amorphous CoFeSiB/Cu/CoFeSiB sputtered multilayers [14, 15]. For a wide film ( $b > 100 \mu\text{m}$  for  $d = 0.5 \mu\text{m}$  or  $b > 10 \mu\text{m}$  for  $d = 0.1 \mu\text{m}$ ), the results are very close to those obtained for an infinite in-plane film. With decreasing  $b$ , the impedance change ratio decreases substantially: for example, for  $100 \mu\text{m}$ -wide films,  $\Delta Z/Z$  reaches more than 300% at a frequency of 150 MHz, whereas its value is only about 70% for  $b = 10 \mu\text{m}$  at this frequency. The decrease in MI is stronger at lower frequencies where the critical width  $b^*$  is larger. In the foregoing example,  $\Delta Z/Z$  recovers up to 200% at a frequency of 900 MHz. As a result, the impedance plots do not show flat regions for small values of  $b$ .

### 3 Asymmetric magnetoimpedance (AMI)

The field behavior of the surface impedance tensor (and voltage responses) is associated with that of the permeability tensor. From (14) and (15) it follows that the permeability parameters  $\tilde{\mu}_{yy}$  and  $\tilde{\mu}_{zy}$  depend on the direction of the static magnetization  $\mathbf{M}_0$ . Therefore, in structures with an asymmetric arrangement of  $\mathbf{M}_0$  (with respect to  $H_{ex}$ ) the impedance also shows an asymmetric behavior (AMI) [18]-[20], [27]. This case is realized in multilayer structures with cross-anisotropy in the presence of the dc bias current  $I_b$ . The other important conclusion is that the components of  $\hat{\zeta}$  have a different symmetry with respect to the dc magnetization: the diagonal components do not change when the direction of  $\mathbf{M}_0$  is reversed, whereas the off-diagonal components do. Then, the voltage response in (6) represented by the combination of  $\zeta_{zz}$  and  $\zeta_{zy}$  can exhibit an asymmetric behavior, which is not associated with that for  $\mathbf{M}_0(H_{ex})$  [27]-[30].

#### 3.1 Dynamical AMI

This section is concerned with the role that the off-diagonal component  $\zeta_{zy}$  plays in producing asymmetry in the total voltage response  $V_f$ . According to (6), the  $\zeta_{zy}$ -contribution to  $V_f$  appears in the presence of the ac bias field  $h_{ex}$ , produced by the coil current, which is the reason to name this type of asymmetry as dynamical AMI. Let us consider a film with a transverse anisotropy, since this case does not have asymmetry in  $\mathbf{M}_0(H_{ex})$ . The transverse domain structure is supposed to be eliminated by the application of

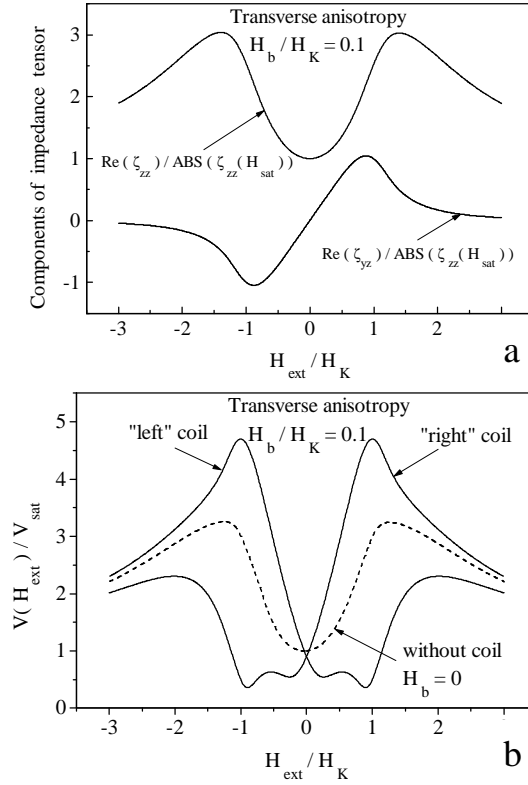


Fig. 5. Surface impedance tensor (a) and voltage response (b) in a film attached to a coil (transverse anisotropy).

a small dc current inducing the transverse bias field  $H_b$ . In this case, the voltage is asymmetrical because  $\zeta_{zz}(H_{\text{ex}}) = \zeta_{zz}(-H_{\text{ex}})$  and  $\zeta_{zy}(H_{\text{ex}}) = -\zeta_{zy}(-H_{\text{ex}})$ .

Figure 5a shows plots of the real parts of  $\zeta_{zz}$  and  $\zeta_{zy}$  vs.  $H_{\text{ex}}$ , at a frequency of 120 MHz. The parameters used correspond to amorphous CoSiB/Cu/CoSiB multilayers:  $2d = 1\mu\text{m}$  and  $2d_1 = d_2$ . The field behavior of the diagonal component  $\zeta_{zz}$  is characterized by two symmetrical peaks when  $H_{\text{ex}}$  is equal to  $1.3H_K$ . On the other hand, the off-diagonal component  $\zeta_{zy}$  is antisymmetric with respect to  $H_{\text{ex}}$ , showing nearly linear behavior in the field range of  $\pm 0.8H_K$ . At the end of this interval it shows either maximum or minimum, and tends to zero as far as the magnetization angle  $\theta$  becomes  $0^\circ$  and  $180^\circ$  which corresponds to  $H_{\text{ex}} = \pm H_{\text{sat}}$ , where  $H_{\text{sat}}$  is the field required to align the dc magnetization  $\mathbf{M}_0$  along the  $z$  axis ( $H_{\text{sat}} > H_K$  in the presence of  $H_b$ ). The value of  $\zeta_{zy}$  at the extremes is of the order of  $\zeta_{zz}(H_{\text{sat}})$  and, consequently according to (6), the application of the ac bias can considerably modify the voltage behavior.

Figure 5 b shows plots of the voltage  $V_f$  as a function of  $H_{ex}$ , calculated in the presence of the ac external field  $h_{ex}$  induced by the coil current. It is seen that  $V_f$  exhibits a considerable asymmetry with respect to  $H_{ex}$ . For comparison, the voltage behavior without  $h_{ex}$  (or without the coil) is shown as well. In this case, the voltage has two symmetrical maximums in line with the  $\zeta_{zz}$  vs.  $H_{ex}$  plot of Figure 5a. Applying  $h_{ex}$  in a positive or negative sense (or using “right” or “left” coil), one of these peaks is suppressed, whereas the other is enhanced and the voltage exhibits essentially asymmetric behavior with an increased sensitivity. A similar result was found in an amorphous wire with circumferential magnetization excited by a current applied to the film and the coil around it [29]. If then two oppositely biased films are connected with the differential amplifier, the output voltage becomes nearly linear in the field range of  $\pm 0.8 H_K$ . It means, that the linearity of the voltage output within the field interval of the order of the anisotropy field can be obtained by applying a much smaller ac field the measure for which is the ac field induced by the ac current flowing in the film.

### 3.2 Static AMI in a film with cross-anisotropy

In this section, AMI due to an asymmetric magnetization reversal is discussed [18]-[20], [27]. The needed magnetic configuration can be realized in the multilayer structure by combining a cross- anisotropy and dc bias current producing a circulatory bias field  $H_b$ . The rotational magnetization process is manifest in Figure 6 where the magnetization plots for different values of  $H_b$  are given. Reversal of  $\mathbf{M}_0$  by rotation is possible, since the magnetization vector during its rotation is held parallel to the surface, without going through high-energy demagnetization states. It is seen that the dc bias causes transition from a symmetric hysteresis curve to an asymmetric anhysteretic one at

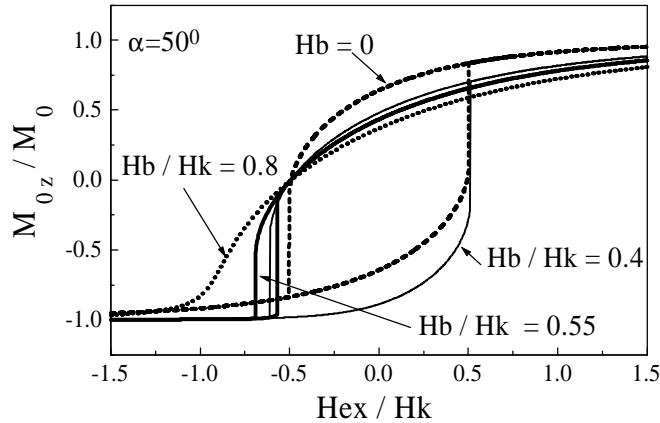


Figure 6. Magnetization curves  $M_{0z}(H_{ex})$  in a wire with a helical anisotropy ( $\alpha = 50^\circ$ ) for different magnitudes of dc bias field  $H_b$ .

$H_b = H^* = H_K \cos \alpha$ . The impedance characteristics reflect this behavior as shown in Figure 7, wherein the plots of  $\zeta_{zz}$  vs.  $H_{ex}$  are given [24]. For  $H_b$  slightly larger than  $H^*$ , the field sensitivity of the impedance change is especially high, and the nominal change can be more than 100% for negative fields, when  $H_{ex}$  is changed by only  $0.1 H_K$ . The other components of the impedance tensor exhibit a similar behavior.

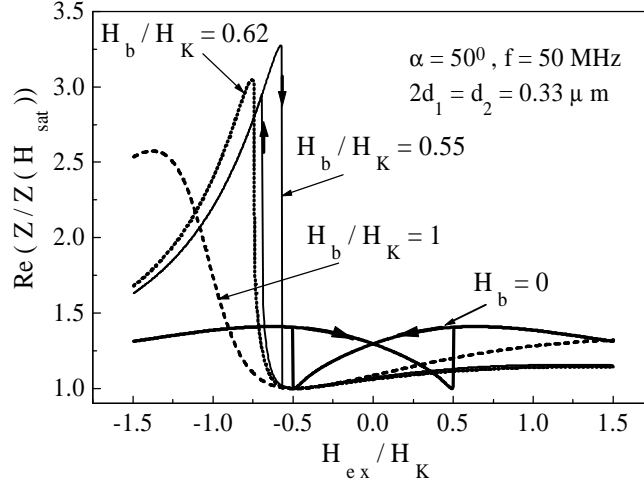


Figure 7. Modifications in the longitudinal impedance  $\zeta_{zz}$  vs.  $H_{ex}$  under the effect of dc bias  $0 \leq H_b/H_K \leq 1$ , when  $\alpha = 50^\circ$ .

### 3. Experimental methods

HP Network Analyzer with a specially designed high frequency measuring cell is used for impedance measurements [32, 33]. The sketch of the measuring system is shown in Figure 8. The analyzer is configured in the two-port option (P1, P2) allowing the  $S_{21}$ -parameter to be measured. This parameter is the ratio of the forward transmission signal  $V_{out}$  to the excitation signal  $V_{in}$ . Depending on the excitation method, the voltage  $V_{in}$  (in the port P1) determines either the ac current  $i$  in the film or current  $i_c$  in the coil. The output voltage  $V_{out}$  (in the port P2) is taken from the film ( $V_{out} = V_f$ ) or from the attached coil ( $V_{out} = V_c$ ). Choosing a certain excitation and measuring channels, all the components of  $\hat{\zeta}$  can be determined. Since the analyzer has an unequal sweep parameter - frequency, the field scanning has to be made by an additional device. The field  $H_{ex}$  is produced from the coil driven by a functional generator and power amplifier. The field was driven in both positive and negative directions to produce the hysteresis plots. The operating processes of the analyzer and functional generator are synchronized by a computer

program. Thus, the functional generator is used as a programmable stepwise dc source to provide the field scans.

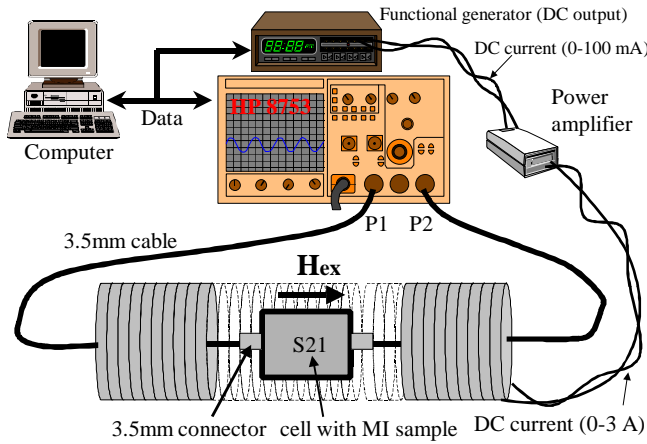


Figure 8. Sketch of the measurement system of  $S_{21}$ -parameter.

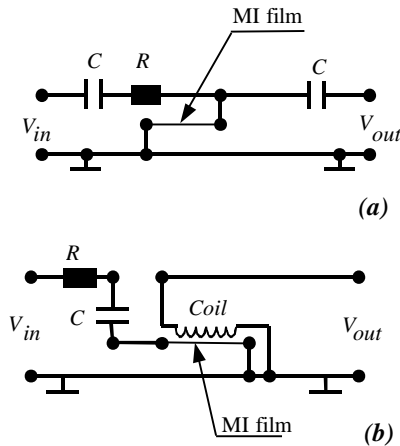


Figure 9. Electronic circuits of the cells to measure diagonal (a) and off-diagonal (b) components of the surface impedance tensor.

The measured sample is placed onto the open-type cell made of copper-coated fiberglass printed circuit board (PCB). All the connection stripes were made 2.8 mm in width to provide the wave impedance of the order of 50-Ohms over a wide range of frequencies. The electrical circuits of the cells for measuring  $V_{ZZ}$  and  $V_{YZ}$  are shown in Figure 9. Blocking capacitor (C) prevents the dc bias current  $I_b$  from entering the analyzer. The cell has input and output 3.5-mm connectors that are connected to the analyzer ports using 3.5-mm to type-N adapters. The microwave track including the cables and adapters was calibrated for the two-port measurements.

The longitudinal diagonal component  $\zeta_{zz}$  is determined by measuring the voltage  $V_f$  across the film excited by an ac current  $i$ . In this case, the cell of Figure 9a is used, for which  $V_{\text{out}} = V_f$ ,  $i_c = 0$ , so that the  $S_{21}$ - parameter is directly proportional to  $\zeta_{zz}$ . It follows from (9) that  $S_{21} = \mathbf{V}_{zz}(H_{\text{ex}})(Al_i/V_{\text{in}})$ . The circulatory diagonal component  $\mathbf{V}_{yy}$  corresponds to the voltage  $V_c$  in the secondary coil mounted on the film which is excited by the primary coil ( $i_c$ ). This case does not present substantial interest and is omitted here. The off-diagonal components  $\mathbf{V}_{zy} = \mathbf{V}_{yz}$  can be determined by measuring the coil voltage  $V_c$  when the film is subjected to current  $i$ , as shown in Figure 9b. In this case,  $V_{\text{out}} = V_c$ ,  $i_c = 0$ , and (9) gives  $S_{21} = \mathbf{V}_{yz}(H_{\text{ex}})(2AbN_2i/V_{\text{in}})$ . Alternatively, the off-diagonal components can be found by measuring the voltage  $V_f$  in the presence of  $i_c$  at the condition  $i = 0$ . If the amplitudes of the ac excitation current (in the film or in the external coil) are chosen to be less than 1 mA, non-linear ac magnetization processes like irreversible domain-wall displacements are not possible. The experimental studies are made with the effect of the dc current which effectively governs the static magnetic structure.

## 5 Film preparation and experimental results

Let us now consider experimental results on MI in thin-film structures. The films are prepared by rf or dc magnetron sputtering methods. The in-plane anisotropy can be established by applying the magnetic field during the deposition. In certain cases, further annealing is required. The induced anisotropy field is in the range of 5-20 Oe. After deposition, the layers can be patterned by conventional photolithographic methods and chemical etching in the needed geometry. Typically, a copper layer is used as the non-magnetic lead. However, it was found that gold may have advantages because it is more reliable and produces much better edge definition when chemically etched.

### 5.1 MI in CoFeSiB/Cu /CoFeSiB multilayers

In the case of CoFeSiB/M /CoFeSiB multilayers (M = Cu, Ag, Au) several microns thick, a very large impedance change (MI ratio) of about 100% can be obtained at a frequency of 1 MHz, whereas the change would not be noticeable in a similar single layer [14, 15]. For small fields  $H_{\text{ex}} \sim 0$ , the impedance magnitude is as low as 0.32-0.36  $\Omega$ , which indicates that it is dominated by the resistance of the M-layer (more than 50 times smaller than that of amorphous layers). The following results were obtained using a copper lead. The MI ratio has two sharp peaks of 145% at  $H_{\text{ex}} = \pm 9$  Oe for CoSiB multilayers, and of 125% at  $H_{\text{ex}} = \pm 18$  Oe for CoFeSiB multilayers. With increasing frequency, the MI ratio increases, reaching a maximum at 10 MHz (340% for CoSiB films). These results are obtained for films having a width of the conductive lead ( $b = 0.5$  mm) more than 10 times larger than the critical length  $b^*$  (taking

$\tilde{\mu}_{yy}=500$ ,  $d_1 = 1.5 \mu\text{m}$  and  $d_2 = 2 \mu\text{m}$ , the parameter  $b^* \approx l = 39 \mu\text{m}$ ), in good agreement with the theoretical results obtained for infinite structures (see Figure 4). As the frequency is further increased, the MI ratio drops rapidly, which can be associated with the experimental technique determining the input impedance of the total system, including that of the lead wires.

A considerable enhancement of the MI effect in multilayers can be achieved by insulator separation between the conductive lead and the magnetic films [15], which further decreases the dc resistance. A CoSiB/SiO<sub>2</sub>/Cu/SiO<sub>2</sub>/CoSiB multilayer exhibited the MI ratio of 620% for 11 Oe.

Morikawa *et al.* [15] investigated the MI effect in CoSiB structures having different inner leads made of silver, copper or titanium. The insertion of a Ag layer (having the smallest resistivity of  $1.62 \mu\Omega\text{-cm}$ ) resulted in the largest MI ratio of 440%, where as the structures having a Ti inner layer with the resistivity of  $47.8 \mu\Omega\text{-cm}$  (only 2.7 times smaller than that of CoSiB) did not exhibit noticeable improvements in MI behavior (as compared with that of a CoSiB layer): the MI ratio was only 50% at a frequency of 100 MHz.

## 5.2. MI in NiFe/M/NiFe multilayers

Permalloy (Ni<sub>80</sub>Fe<sub>20</sub>) having almost no magnetostriction is an excellent soft magnetic material. The resistivity of a NiFe layer is  $20 \mu\Omega\text{-cm}$  which is about 12 times larger than that of Cu, Ag, or Au. It implies that this material is also suitable for multilayer MI, as was proposed by Hika *et al.* [16] Here we present new results on MI in NiFe/Au/NiFe multilayers obtained for various geometries and frequency ranges. The films were deposited on a glass substrate in the presence of the dc field of about 100 Oe. The film geometry has been proven to affect greatly the dc magnetic structure. Taking the length of MI element in the range of 2-5 mm, and its thickness  $d < 2 \mu\text{m}$ , we found that longitudinal anisotropy is induced if the film width is smaller than  $200 \mu\text{m}$ .

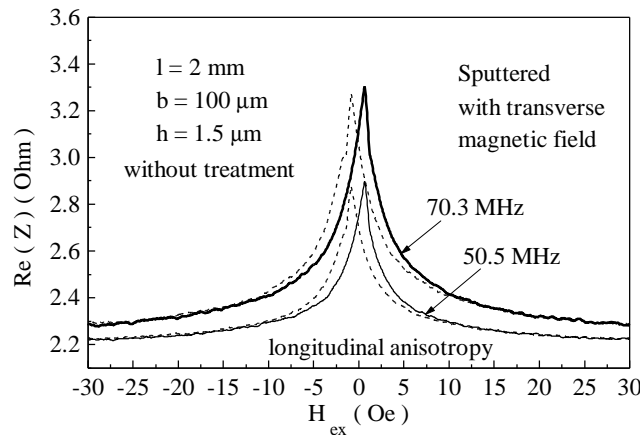


Figure 10. Real part of the impedance vs. field in FeNe/Au/FeNe films with longitudinal anisotropy for  $b=100\mu\text{m}$ . Dashed curves correspond to  $H_{\text{ex}}$  reversed from negative to positive direction.

After deposition, annealing was needed to establish the anisotropy axes in the transverse direction. This effect is due to the tension existing at glass/metal interface. With a proper choice of glass substrate, the tension can be released by annealing, so that the anisotropy returns to the direction established by the magnetic field applied during the deposition process.

Figure 10 shows plots of the real part of  $Z$  as a function of  $H_{ex}$  for films with a longitudinal anisotropy. For films with larger widths ( $b > 100 \mu\text{m}$ ), the MI ratio reaches about 50% at frequencies of 50-70 MHz. In narrower films ( $b < 50 \mu\text{m}$ ), higher frequencies are needed to obtain large MI ratios, as shown in Figure 11. This agrees well with theory (compare with Figure 4)

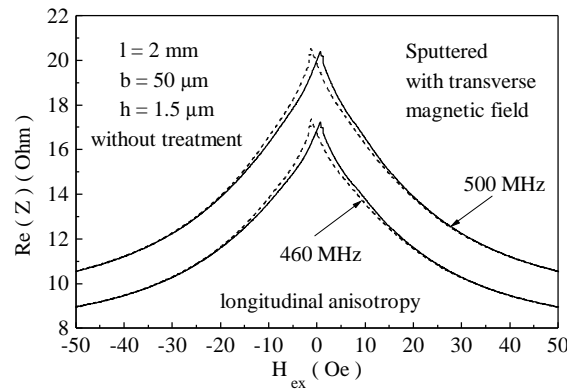


Figure 11. Real part of  $Z$  vs.  $H_{ex}$  for FeNe/Au/FeNe films with longitudinal anisotropy;  $b=50 \mu\text{m}$ , and  $f=400\text{-}500 \text{ MHz}$ . Dashed curves correspond to  $H_{ex}$  reversed from negative to positive direction.

Figure 12 shows plots of the real part of  $Z$  as a function of  $H_{ex}$  for films with transverse anisotropy. These films were deposited in the presence of a dc magnetic field. After deposition, they were annealed to release the stress and establish transverse anisotropy. On comparing with the data obtained for the case of longitudinal anisotropy, it is seen that the transverse anisotropy results in much higher sensitivity. The field characteristics alter as well, displaying two symmetrical maximums when the external field equals the anisotropy field (about 10 Oe). The MI ratio and sensitivity increase with frequency reaching 240% and 24%/Oe, respectively, at frequency of 500 MHz.

### 5.3 Asymmetric MI (AMI)

We have considered miniature multilayer structures exhibiting the MI sensitivity in the range of 25%/Oe, which makes them very attractive for sensor application. One more important parameter of sensor operation is linearity. On the other hand, the MI characteristics seen in Figures 10-12 are not only non-linear, but also shaped in a way that the operation near zero-field point can present serious problems. Generally, a dc bias field can be used to set properly the operating point on the MI characteristics.

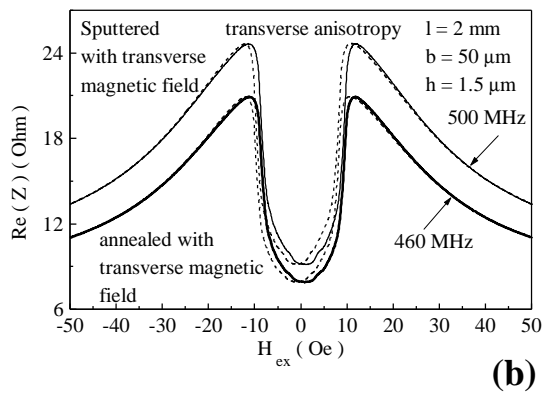
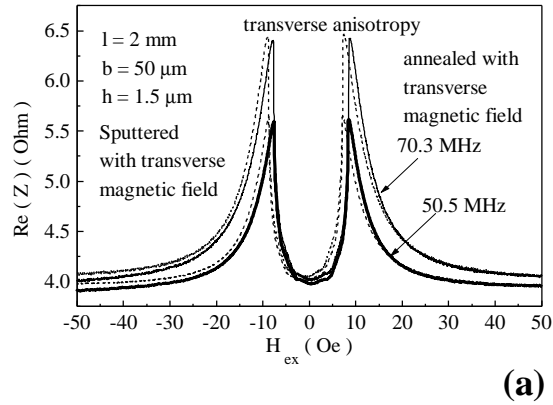


Figure 12. Real part of  $Z$  vs.  $H_{ex}$  for FeNe/Au/FeNe films with transverse anisotropy. (a)  $f=50-70$  MHz ; (b)  $f=450-500$  MHz. Dashed curves correspond to  $H_{ex}$  reversed from negative to positive direction.

In fact, biasing produces asymmetry with respect to the sensed field  $H_{ex}$ . To simplify the sensor design, it would be preferable to utilize intrinsic AMI characteristics as analyzed in Section 3. Two types of AMI effects can be realized in multilayers. The first one requires asymmetrical static magnetic configuration as that of cross-anisotropy multilayers [34]. The second type, so-called dynamical AMI, is realized in film-coil structure.

First we consider the results obtained in cross-anisotropy films of the composition  $Co_{70.2}Fe_{7.8}B_{22}/Cu/Co_{70.2}Fe_{7.8}B_{22}$ . The films were made on a glass substrate by dc sputtering. The sputter rates were 17 nm/min and 50 nm/min, background pressure and Ar gas pressure were  $3 \cdot 10^{-5}$  Pa and 0.1 Pa, respectively. During the deposition, the temperature of the substrate was  $35^{\circ}C$ , and a constant magnetic field of 200 Oe was applied in the transverse direction to the MI element in order to add uniaxial anisotropy. Finally, crossed anisotropy was induced in the sample by current annealing (30 mA) in

longitudinal field of 11.8 Oe at a temperature of 215°C. The sample in-plane view and magnetic configuration is shown in Figure 11. The thickness of all the layers is 0.5 $\mu$ m. The anisotropy axes  $n_K$  in the upper and bottom layers are at approximately 67° to the  $z$  axis, which was estimated from the dc magnetization loop measurements.

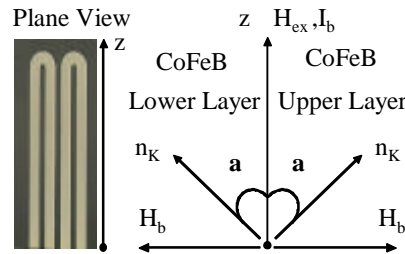


Figure 13. Plane view, principal dimensions and quantities for CoFeB/Cu/CoFeB films.

The measured results for impedance are given in Figures 14-16. At low MHz frequencies (Figure 14) the application of dc bias current  $I_b$  shifts the central peak seen at  $I_b = 0$  towards negative values of  $H_{ex}$ , which is consistent with the dominant domain wall dynamics contribution to the ac permeability. The sensitivity is nearly 20%/Oe. With increasing frequency, the field characteristics change, as is evident in Figure 15, since the rotational processes become more significant. Figure 16 shows the differential characteristic from two oppositely biased MI films, which has near linear region in the field interval of  $\pm 5$  Oe. This demonstrates the achieved linearity without using dc bias field.

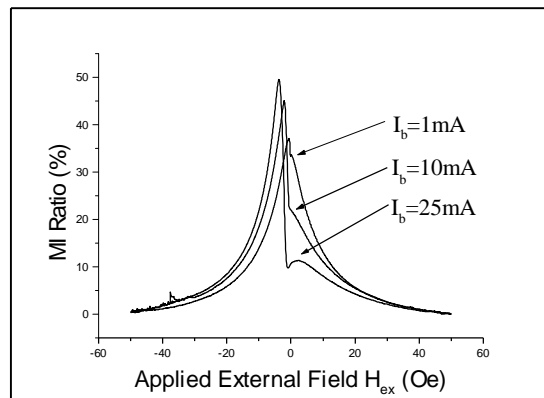


Figure 14. Magnitude of  $Z$  vs.  $H_{ex}$  for  $I_b$  as a parameter in CoFeB/Cu/CoFeB multilayers at frequency 10 MHz.

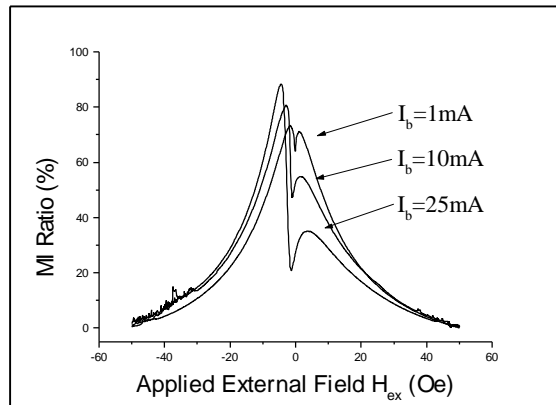


Figure 15. Magnitude of  $Z$  vs.  $H_{ex}$  for  $I_b$  as a parameter in CoFeB/Cu/CoFeB multilayers at frequency 40 MHz.

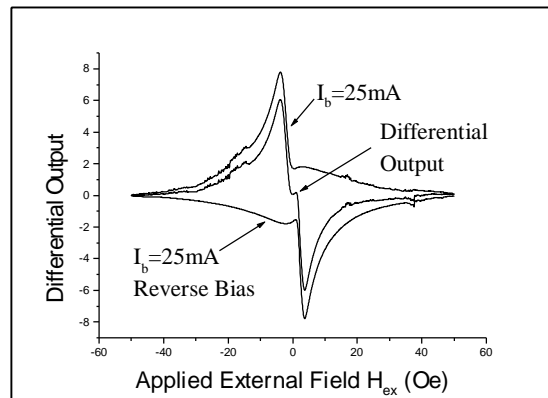


Figure 16. Differential voltage response at frequency 10 MHz, obtained using two oppositely biased films with MI characteristics given in Figure 14.

Very promising results on AMI have been obtained using NiFe/Au/NiFe multilayers deposited in the presence of a dc magnetic field. After the deposition of the bottom layer, the substrate was rotated by 90 degrees; therefore, the two magnetic layers were deposited in cross magnetic fields. After releasing stress by annealing, a cross-anisotropy film was finally produced. The AMI characteristics obtained in the presence of a dc bias current  $I_b$  are given in Figure 17. In this case, a well-pronounced asymmetry is obtained at high frequencies (in the 30-70 MHz range) is due to the rotational ac dynamics. Although the field sensitivity in the presence of  $I_b$  can be very high, there is a substantial hysteresis. The obtained results on cross-anisotropy films display a very good compromise on size, sensitivity, and linearity.

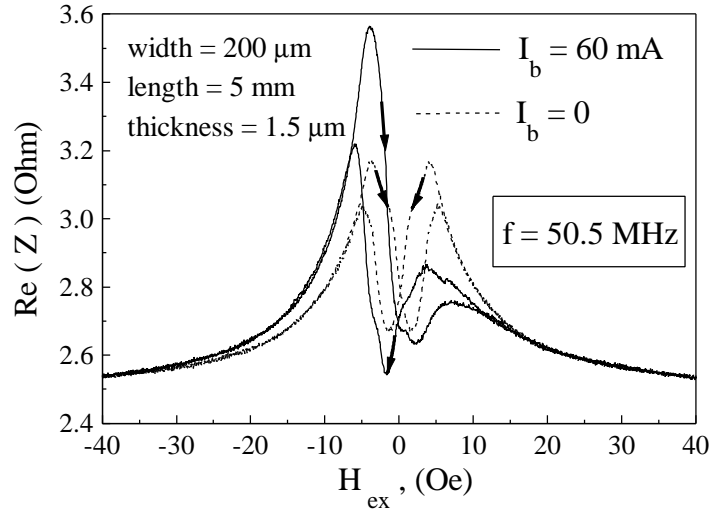


Figure 17. Real part of impedance  $\text{Re}(Z)$  vs.  $H_{\text{ex}}$  in NiFe/Au/NiFe multilayers with cross-anisotropy at frequency 50.5 MHz for two values of bias current  $I_b$ : 0 and 60 mA.

## 6 Practical MI sensor design

Typically, MI sensors are based on diagonal impedance characteristics. A complicated biasing technique is then needed to properly set the operational regime for linear sensing. If AMI effect is used, then two film-elements are needed to obtain a differential response. Several sensor circuits have been proposed by Mohri and co-authors [5,34], using either sinusoidal or pulsed excitation of an amorphous wire MI element. These circuits can be implemented also with thin films. Further development of MI sensors have shifted to the utilization of off-diagonal impedance components [35], when the output is taken as a coil voltage. In this case, circuit design can be simplified and sensor parameters (such as linearity and temperature stability) are improved. In this section, we focus on principles for using the off-diagonal impedance for sensor applications.

Let us consider a circuit where the off-diagonal response (proportional to  $\zeta_{yz}$ ) is taken from the pick-up coil, and a single MI element is used. The principle electronic circuit is shown in Figure 19. The C-MOS IC multivibrator (with invertors Q) in this circuit produces smoothed rectangular pulses at a frequency of a few hundred kHz. After passing through the differential circuit (C1-R1), the pulse is sharpened and high-frequency harmonics exist in its spectrum. Pulse excitation is preferred over sinusoidal excitation for several reasons, such as simplicity of electronic design, low cost components and high stability. In addition, the pulse spectrum contains a dc offset (zero harmonic)

that provides the dc bias required for the existence of the off-diagonal response. Thus, the pulse circuit produces both the high-frequency excitation

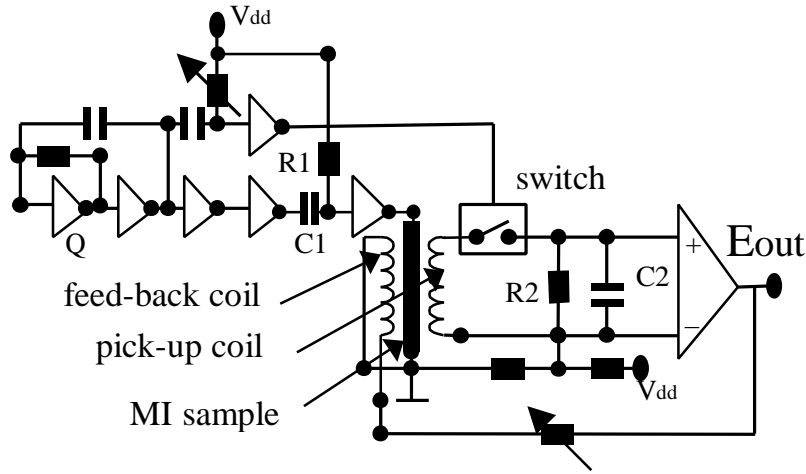


Figure 18. Electronic circuit of a linear sensor using the off-diagonal impedance for a linear sensor. It comprises a C-MOS IC multivibrator with inverters (Q), a differential circuit (C1-R1), analog synchronised switch, rectifier (R2-C2), a differential amplifier, and negative feed-back.

and dc bias. The ac off-diagonal pulsed response  $V_c$  is taken from the pick-up coil using the analog synchronized switch, and converted by the rectifier (R2-C2). The synchronous rectification suppresses the noise that appears during the rectification process and produces a quasi-dc voltage of the magnitude proportional to the original pulse amplitude. Thereafter, the rectified voltage is amplified. This amplified signal is characterized by an amplitude, and a sign, both of which are sensitive to the dc external magnetic field  $H_{ex}$  since the off-diagonal response is used. Thus, a near-linear output voltage signal is obtained without use of negative feedback, which, however, can be added to further improve linearity. The circuit proposed by Kawajiri *et al.* [35] uses two MI elements and two analog switches to create a balanced circuit with very high temperature stability.

Another method for obtaining a linear response is provided by so-called mixed excitation [27]-[30], wherein an MI film with transverse anisotropy (or wire with the circumferential anisotropy) is excited by both the ac longitudinal current  $i$  and the ac longitudinal magnetic field  $h_{ex}$ . The excitation can be pulsed or sinusoidal. For sinusoidal excitation, an additional dc bias current is required to generate off-diagonal surface impedance. The field  $h_{ex}$  can be induced by a coil mounted around the sample and connected in series. The output signal  $V_f$  is measured across the MI sample. As can be deduce from (6), the ac response is formed by the sum of the diagonal

$\zeta_{zz}(H_{ex})$  and off-diagonal  $\zeta_{zy}(H_{ex})$  impedance components with corresponding coefficients. Since  $\zeta_{zz}(H_{ex})$  and  $\zeta_{zy}(H_{ex})$  are symmetric and

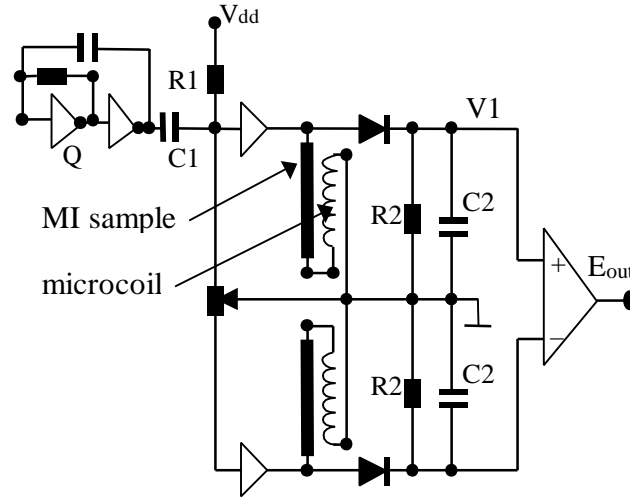


Figure 19. Electronic circuit of a linear sensor using mixed excitation. The MI samples are excited by both the ac longitudinal current  $i_z$  and the ac longitudinal magnetic field  $h_{ex}$ . The output signals are measured across the MI samples.

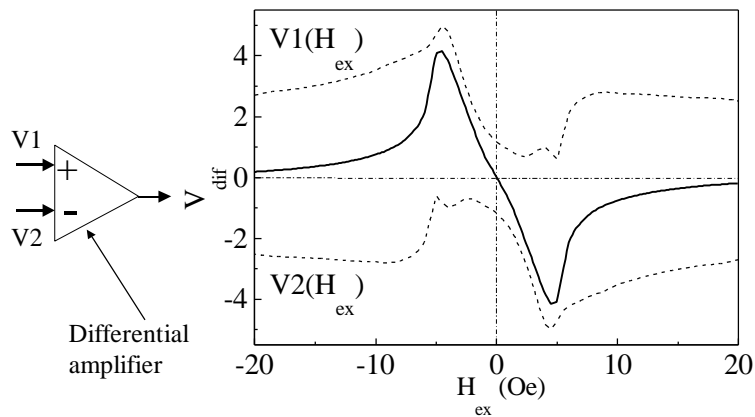


Figure 20. Principle underlying the near-linear field response of a differential circuit. Two voltage responses  $V_1$  and  $V_2$  produced with opposite ac bias are added together in the differential amplifier.

antisymmetric, respectively, the field dependence of the output voltage magnitude  $|V_f|$  on  $H_{ex}$  is asymmetric. The linear sensor circuit is shown in Figure 20. The signals  $V1(H_{ex})$  and  $V2(H_{ex})$ , taken from the two MI

sensors with reverse asymmetries, are detected in a differential sense to produce the total linear field response  $V_{\text{dif}}(H_{\text{ex}})$ , as shown in Figure 20. Therefore, no additional dc bias field is required in this case to produce a linear output response as well.

## 7. Conclusions

The following conclusions emerge from the developments presented in this chapter:

1. The MI effect in multilayers, which has two soft ferromagnetic films (F) sandwiching a highly conductive lead (M), has significant advantages over that of a single layer. First, the MI ratio is several times greater ranging within 100 - 600 % for films of 1-10  $\mu\text{m}$  thickness. Second, the impedance shows large changes (50 -100 %) at relatively low frequencies ( $\sim 1\text{MHz}$  for this case) when the skin effect is not substantial.

2. Theoretical analysis has been developed for a 3-layer structure (F/M/F) with magnetic films having an in-plane anisotropy of a “spiral” type. For a considerable conductivity difference between the layers F and M, the inductance of the magnetic films is the main contributor to the system impedance at relatively low frequencies. The voltage response is linearly proportional to the permeability tensor, which can be extremely sensitive to the longitudinal sensed field. The theory accounts for the influence of the in-plane dimensions on the MI ratio, yielding a quantitative agreement with the experiment.

2. Consideration of asymmetric MI requires an approach involving of surface impedance tensor. Regarding the conceptual aspects, it has been demonstrated that there are two principally different mechanisms of AMI. One is related to the asymmetric static magnetization reversal, and the other is caused by the dynamical cross-magnetization process represented by the off-diagonal impedance.

- 4 The application of MI multilayers for new sensitive and quick response micromagnetic sensors is at an early stage of its development. However, it can be expected that significant technical achievements in this field will be made in the foreseeable future. The tensor character of the surface impedance opens new principles for linear sensors designed to take advantage of antisymmetric off-diagonal impedance.

## References

- [1] D. Robbes, C. Dolabdjian, S. Saez, Y. Monfort, G. Kaiser and P. Ciureanu, Highly sensitive uncooled magnetometers: state of art. Superconductive magnetic Hybrid magnetometers, an alternative to SQUIDS?, *IEEE Trans App Superconductivity*. **11** (2001), 629-634.
- [2] D.J. Mapps, Magnetoresistive sensors, *Sens Actuat A: Phys* **59** (1997), 9-19.
- [3] F. Primdahl, The fluxgate mechanism, part I: The gating curves of parallel and orthogonal fluxgates, *IEEE Trans Magn* **6** (1970), 376-383.
- [4] K. Mohri, L.V. Panina, T. Uchiyama, K. Bushida and M. Noda, Sensitive and quick response micro-magnetic sensor utilizing magneto-impedance in co-rich amorphous wires, *IEEE Trans Magn* **31** (1995), 1266-1275.
- [5] K. Mohri, T. Uchiyama and L.V. Panina, Recent advances of micro magnetic sensors and sensing application, *Sens Actuat A: Phys* **59** (1997), 1-8.
- [6] M. Vazquez and A. Hernando, A soft magnetic wire for sensor applications, *J Phys D: Appl Phys* **29** (1996), 939-949.
- [7] L.V. Panina and K. Mohri, Magneto-impedance effect in amorphous wires, *Appl Phys Lett* **65** (1994), 1189-1191.
- [8] L.V. Panina, K. Mohri, K. Bushida and M. Noda, Giant magneto-impedance and magneto-inductive effects in amorphous alloys, *J Appl Phys* **76** (1994), 6198-6203.
- [9] R.S. Beach and A.E. Berkowitz, Giant magnetic-field dependent impedance of amorphous FeCoSiB wire, *Appl Phys Lett* **64** (1994), 3652-3654.
- [10] R.S. Beach and A.E. Berkowitz, Sensitive field-dependent and frequency-dependent impedance spectra of amorphous FeCoSiB wire and ribbon, *J Appl Phys* **76** (1994), 6209-6213.
- [11] J. Valazquez, M. Vazquez, D.X. Chen and A. Hernando, Giant magnetoimpedance in nonmagnetostrictive amorphous wires, *Phys Rev B* **50** (1994), 16737-16740.
- [12] L.V. Panina, K. Mohri, T. Uchiyama, K. Bushida and M. Noda, Giant magneto-impedance in co-rich amorphous wires and films, *IEEE Trans Magn* **31** (1995), 1249-1260.

- [13] D.P. Makhnovskiy, L.V. Panina and D.J. Mapps, Field-dependent surface impedance tensor in amorphous wires with two types of magnetic anisotropy: helical and circumferential, *Phys Rev B* **63** (2001), 144424-144441.
- [14] T. Morikawa, Y. Nishibe, H. Yamadera, Y. Nonomura, M. Takeuchi and Y. Taga, Giant magneto-impedance effect in layered thin films, *IEEE Trans Magn* **33** (1997), 4367-4369.
- [15] T. Morikawa, Y. Nishibe, H. Yamadera, Y. Nonomura, M. Takeuchi, J. Sakata and Y. Taga, Enhancement of giant magneto-impedance in layered film by insulator separation, *IEEE Trans Magn* **32** (1996), 4965-4967.
- [16] K. Hika, L.V. Panina and K. Mohri, Magneto-impedance in sandwich film for magnetic sensor heads, *IEEE Trans Magn* **32** (1996), 4594-4596.
- [17] L.V. Panina and K. Mohri, Magneto-impedance in multilayer films, *Sens Actuat A: Phys* **81** (2000), 71-77.
- [18] D.P. Makhnovskiy, A.S. Antonov, A.N. Lagar'kov and L.V. Panina, Field-dependent surface impedance of a bilayer film with an antisymmetric bias magnetization, *J Appl Phys* **84** (1998), 5698-5702.
- [19] L.V. Panina, D.P. Makhnovskiy and K. Mohri, Analysis of magneto-impedance in multilayers with cross-anisotropy, *J Mag Soc Jpn*, **23**, (1999), 925-931.
- [20] D.P. Makhnovskiy, L.V. Panina, A.N. Lagar'kov and K. Mohri, Effect of antisymmetric bias field on magneto-impedance in multilayers with crossed anisotropy, *Sens Actuat A: Phys* **81** (2000), 106-110.
- [21] L.V. Panina, D. Zarechnuk, D.P. Makhnovskiy and D.J. Mapps, Two-dimensional analysis of magnetoimpedance in magnetic/metallic multilayers, *J Appl Phys* **89** (2001), 7221-7223.
- [22] V. Korenivski, GHz magnetic film inductors, *J Magn Magn Mater* **215-216** (2000), 800-806.
- [23] A. Sukstanskii, V. Korenivski and A. Gromov, Impedance of a ferromagnetic sandwich strip, *J Appl Phys* **89** (2001), 775-786.
- [24] D.P. Makhnovskiy and L.V. Panina, Size effect on magneto-impedance in layered films, *Sens Actuat A: Phys* **81** (2000), 91-94.
- [25] A. Paton, Analysis of the efficiency of thin-film magnetic recording heads, *J Appl Phys* **42** (1971), 5868-5870.

- [26] R. W. Cross, S.E. Rassek, S.C. Sanders, M.R. Parker, J.A. Barnard and S.A. Hossain, Size and self-field effects in giant magnetoresistive thin-film devices, *IEEE Trans Magn* **30** (1994), 3825-3827.
- [28] L.V. Panina, D.P. Makhnovskiy and K. Mohri, Mechanism of asymmetrical magnetoimpedance in amorphous wires, *J Appl Phys* **85** (1999), 5444-5446.
- [29] D.P. Makhnovskiy, L.V. Panina and D.J. Mapps, Asymmetrical magneto-impedance in a sandwich film with a transverse anisotropy using an AC bias, *J Magn Mater* **215** (2000), 629-633.
- [30] K. Gunji, L.V. Panina and K. Mohri, Asymmetrical magneto-impedance in amorphous wires with helical current excitation, *J Mag Soc Jpn* **21** (1997), 793-797.
- [31] D.P. Makhnovskiy, L.V. Panina, D.J. Mapps, Asymmetrical magnetoimpedance in as-cast CoFeSiB amorphous wires due to ac bias, *Appl. Phys. Letters* **77** (2000), 121-123.
- [32] D.P. Makhnovskiy, L.V. Panina and D.J. Mapps, Measurement of field-dependent surface impedance tensor in amorphous wires with circumferential anisotropy, *J Appl Phys* **87** (2000), 4804-4806.
- [33] D.P. Makhnovskiy, L.V. Panina and D.J. Mapps, Surface impedance tensor in amorphous wires with helical anisotropy: Magnetic hysteresis and asymmetry, *J Appl Phys* **89** (2001), 7224-7226.
- [34] K. Ueno, H. Hiramoto, K. Mohri, T. Uchiyama, and L.V. Panina, Sensitive asymmetrical MI effect in crossed anisotropy sputtered films, *IEEE Trans Magn* **36** (2000), 3448-3450.
- [35] K. Mohri, T. Uchiyama, L.P. Shen, C.M. Cai and L.V. Panina, Sensitive micro magnetic sensor family utilizing magneto-impedance (MI) and stress-impedance (SI) effects for intelligent measurements and controls, *Sens Actuat A: Phys* **91** (2001), 85-90.
- [36] N. Kawajiri, M. Nakabayashi, C.M. Cai, K. Mohri and T. Uchiyama, Highly stable micro sensor using C-MOS IC multivibrator with synchronous rectification, *IEEE Trans Magn* **35** (1999) 3667-3669.